Fragmentation Instabilities of a Liquid Drop Falling in a Miscible Fluid

P. K. Buah-Bassuah[*,1], S. Residori[2] and F. T. Arecchi[3]
[1] *Laser and Fibre Optics Centre, Department of Physics, University of Cape Coast, Cape Coast, Ghana*
[2] *Institut Non Linéaire de Nice,1361 Route des Lucioles, Valbonne-Sophia Antipolis, France*
[3] *Physics Department, University of Florence and CNR-Istituto Nazionale di Ottica Applicata, Largo Enrico Fermi 6, Florence, Italy*

We report a set of experimental investigations on the break-up of a liquid drop when falling in a miscible solvent, with the density difference being positive, or negative, or zero. Non-dimensional numbers, derived from the characteristic times of the drop evolution, account for the hydrodynamic instabilities and the self-similar character of the fragmentation process. The role of the initial surface tension at the air-drop interface is explored, leading to scaling laws for the drop volume V and the various height h reached by the drop before it fragments into smaller droplets. From the first break-up to the onset of diffusion, the fragmentation process is shown to have a fractal structure, which is associated to universal power laws for h and V during the dynamical processes associated to the break-up phenomena.

1. Introduction

The break-up process of a drop falling in a miscible solvent was first considered qualitatively by [1]. The experimental investigation of such transient dynamical phenomena reveals the competition between the break-up induced by the non-linear hydrodynamic processes and the local damping due to diffusion of the velocity and concentration gradients [1]. Indeed, the dynamics of fragmentation of such a liquid drop falling into a miscible fluid is ruled by interfacial surface tension associated with density difference, known as Rayleigh-Taylor instability [2] (R-T), and the presence of velocity gradients between the drop and the fluid composing the solvent, which is referred to as Kelvin-Helmholtz (K-H) instability [2,3]. In order to understand in detail the competition between the hydrodynamic instability and the diffusional mixing, different miscible fluids of different compositions are tested. It is shown that the fragmentation process is ruled by two non-dimensional numbers, namely the Fragmentation number F and Schmidt number S, derived from three characteristics times of the drop dynamics: $F = g\Delta\rho V/\mu D$ and $S = \nu/D$, where g is the gravity acceleration, $\Delta\rho$ is the density difference between the drop and the solvent, V the drop volume, $\nu = \mu/\rho$ the kinematic viscosity, μ and ρ the viscosity, respectively, the density of the solvent, and D the diffusion constant of the drop into the solvent [4,5].

By changing the fluid parameters, such as μ, ρ and D for different drop volumes V, the drop break-up can be observed at different cell heights h. However, by controlling $\Delta\rho, V$, and μ at fixed D, it was found that above a critical value F_c of the Fragmentation number, the drop breaks into a number N_1 of fragments, which increases as S decreases. If each of the N_1 secondary droplet has an individual Fragmentation number still higher than F_c, then a second break-up occurs. For the fluid mixtures considered, the fragmentations went not beyond three steps, since at the third stage the tertiary droplets (with $N = N_1N_2$, N_2 being the number of fragmentations of each one of the N_1 secondary droplets) were small enough to have an individual fragmentation number below F_c [4].

Inferring from the experimental observations, it can be explained that the K-H instability is predominant in the early stages of the process, when the drop is deposited on the free surface of the solvent and, upon falling, develops a vortex ring expanding horizontally. Once the ring is formed, R-T instability sets in at the interface due to the density difference between the ring and the solvent. Behind the ring, the drop fluid leaves a membrane that looks like a turban, in concave shape in the case of positive density difference and in a reversed convex shape in the case of negative density difference. At this stage, an undulation begins to be amplified at the interface along the torus until a break-up into secondary droplets takes place. The process replicates itself if the velocity gradient

*buahbass@hotmail.com

and the density difference are large enough for the Fragmentation number to be greater than its critical value. The process stops as viscous dissipation and concentration diffusion overcome the K-H and R-T mechanisms.

In this paper, three experimental investigations are presented, by focusing on the fluid parameters. Depending on the density difference $\Delta\rho$ between the drop and the solvent we have studied the following scenarios: 1. $\Delta\rho$ positive (that is, the drop is heavier than the solvent) and the subsequent break-up process associated with fractalization until diffusion sets in; 2. $\Delta\rho$ zero (that is, the drop and the solvent are made of the same fluid) and investigation of the role of initial surface tension of the drop against air; 3. $\Delta\rho$ negative (that is, the solvent is heavier than the drop), showing an inversion of velocity with the drop fragments going upwards to the free surface of the solvent.

2. The Experimental Setup and Measurements

The experimental set up, as shown in Fig. 1, consists of a glass cell with a base of 10x10 cm^2 and 40 cm high, filled with the solvent and mounted on a rigid metallic support. On top of the cell is mounted a microsyringe that releases a drop close to the centre of the free surface at zero initial velocity and $h = 0$ (h being the downward vertical coordinate within the solvent). The behaviour of different fluid mixtures, namely the solvent being made up of distilled and purified water doped at $0, 10, 15, 25\%$ glycerin and the drop made up of distilled and purified water with a glycerin concentration varying from 0 to 40%, is investigated.

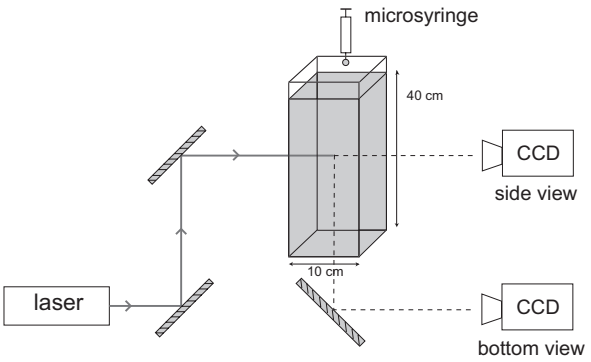

FIG. 1: Experimental setup: a solid state laser beam ($\lambda = 532\ nm$) illuminates laterally the cell; fluorescence from the drop is recorded by a charge-coupled device (CCD) camera.

The cell was illuminated by diode pumped solid state laser ($\lambda = 532\ nm$). The drop was seeded with a small amount of sodium fluorescein dye ($10^{-9}\ mol/litre$), so that the emitted fluorescence from the laser illumination would enable its visualization. Side and bottom views of the drop inside the solvent are imaged by an objective onto a CCD camera consisting of 512 x 512 pixels, then registered by a video recorder and digitized by a frame grabber with 8-bit resolution. The CCD camera has a standard video acquisition rate, with each frame lasting for 40 ms. The objective of the camera is adjusted in such a way that the focal length is sufficiently long to obtain sliced images at different heights through the cell. The experiment was carried out for different drop sizes corresponding to a drop volume ranging between 1 to 24 μl.

2.1. The drop break-up

Demonstrating the break-up phenomena with different $\Delta\rho/\mu$, V and for $\Delta\rho > 0$, (that is the drop is heavier than the solvent), the drop composition of 40% glycerin, 60% of water and solvent composition of 25% glycerin, 75% water were chosen and the drop volume was varied from 1 to 24 μl. Typical experimental pictures of bottom views of multiple fragments after the first break up are shown in Fig. 2 and side views of successive multiple fragmentations are shown in Fig. 3. Specifically, with the drop of 2 μl and 15% glycerin mixed with 85% of water falling in the same solvent composition (25% glycerin and 75% water), that is, the solvent is heavier than the drop, a typical behaviour of density difference less than zero, $\Delta\rho < 0$, is shown in Fig. 4. The fast injection of the drop, the ring formation, its undulation and subsequent fragmentation into four droplets, then rising up towards the free surface of the surface are illustrated

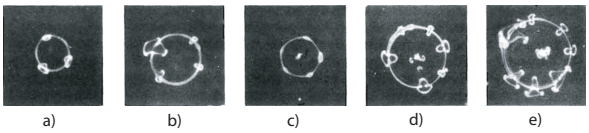

FIG. 2: Experimental snapshots showing examples of multiple fragments after the first break- up of the torus into: a) three, b) four, c) five, d) six, and e) seven fragments.

In order to observe conveniently the initial stages of the falling drop phenomena, the drop evolution is slowed down by playing on the quantity $\Delta\rho/\mu$. A drop of 90% glycerin and 10% water with a volume of 1 μl and seeded with carbon particles (size $\sim 70\ \mu m$) is made to fall in solvent of 60%

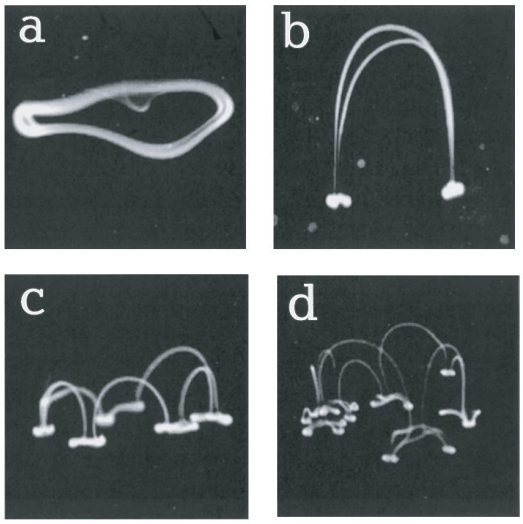

FIG. 3: Side views of the drop falling in a lighter solvent; a) the drop, initially spherical, has become a torus; some regions with greater density give rise to successive fragmentations, b) two or c) six, depending on the fluid parameters. In d), the six secondary droplets of panel c) split again during the last stage of fragmentation.

glycerin and 40% water. The falling drop generates growing vorticity and shear at the interface between the two fluids. Thus, inside the cell the drop transforms into a ring shape leaving behind a concave membrane attached to the torus to form a turban. This is evident in Fig. 4 and Fig. 5, suggesting that the turban instability manifests itself in the drop break-up process independently of the type of density difference.

The cascade of fragmentations as seen in Fig. 3 stops after three steps, when the radius of the tertiary droplets has become so small that diffusion sets in and takes over the process. Such observations of drop break-up and its disappearance by diffusion is assigned by the non-dimensional number F. This is expressed as the ratio of the two characteristic times of the drop evolution. The falling drop behaves in such a way that the downward force due to gravity is proportional to the density difference $\Delta\rho$ between the two fluids. After a transient regime, an equilibration time $\tau' = \rho r^2/\mu$ (where ρ is the drop density, r the drop radius and μ the surrounding fluid viscosity) is reached, when the gravity force is compensated by the Stokes force that subsequently is proportional to the product of the drop velocity and viscosity of the surrounding fluid. Thus, in the sedimentation regime, the asymptotic velocity $v_\infty \sim g\Delta\rho r^2/\mu$ is reached.

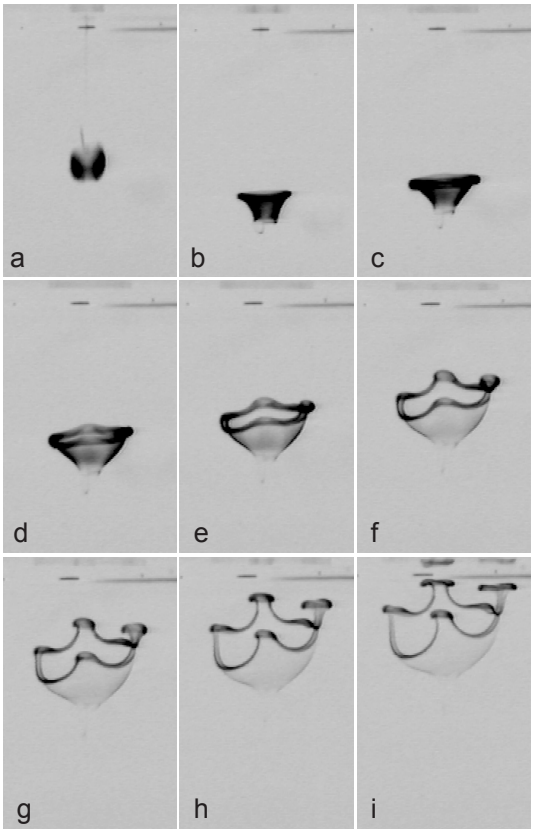

FIG. 4: Side views of the drop falling in a heavier solvent; a) the drop injection ($t = 0.08\ s$), b)c) the ring formation ($t = 0.20, 0.32\ s$), d) the development of the turban ($t = 0.44\ s$), e) f) onset of the fragmentation ($t = 0.56, 0.68\ s$), g) h) i) rise up of the fragments ($t = 0.80, 0.92, 1.04\ s$).

Therefore, the fragmentation of a drop falling with the asymptotic velocity implies the onset of a circular velocity, and this requires at least a time τ_1 corresponding to the transfer of v_∞ across the drop radius, that is, $\tau_1 = r/v_\infty \sim \mu/(\Delta\rho g r)$. Such a process is counteracted by diffusion, which takes place over the time τ. The fragmentation then stops at a radius where τ_1 becomes longer than a fixed fraction of τ, denoted by $\tau_2 = r^2/D$ and assigned as the diffusion time. The Fragmentation number F is thus defined as [4]

$$F = \frac{\tau_2}{\tau_1} = g\frac{\Delta\rho}{\mu}\frac{V}{D} \tag{1}$$

and fragmentation takes place when F is greater than F_c, the critical Fragmentation number.

When initial drops with $F > F_c$ undergo fragmentation, then the daughter drops may or not fragment again, depending if their volume is such

that F is greater or smaller than F_c. Plotting V/D against $\Delta\rho/\mu$, F_c was measured to be $(2.8 \pm 0.1)\text{x}10^5$, as derived from the boundary line distinguishing between the break-up and non break-up of the torus developing from drops with various fluid compositions [4]. F is found to be independent of the nature of the two miscible fluids. However, it was observed that τ' is smaller than τ_1 and τ_2. Thus, within the τ_1 and τ_2 interval, there is a break up time τ_{bu} for the first fragmentation to take place. It was assumed that τ' is negligible in the process.

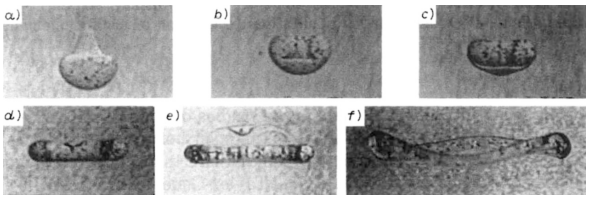

FIG. 5: Evolution of a falling drop with $r = 0.29\ cm$ and $\Delta\rho = 0.0789\ g/cm^3$. a)-f) Sequence of lateral views taken at the following positions from the free surface and times from the deposition: a) 2.0 cm, 1.05 s; b) 6.0 cm, 3.03 s; c) 8.0 cm, 4.0 s; d) 10.0 cm, 5.2 s; e) 13.0 cm, 7.34 s; f) 16.0 cm, 10.0 s. Panel e) shows the appearance of the turban instability and panel f) the break-up of the torus induced by the R-T instability.

Considering the horizontal fragments, as in Fig. 2, it is observed that two forces, namely the gravity and the viscous drag, act on the spherical drop falling in a quiescent liquid. The net force is given by the sum of the buoyancy force, $F_b \propto \Delta\rho V g$, and a drag term, $F_d \propto \mu r v$. The reference time is $\tau' = Mv/F_d$ with M the drop mass $M = \rho V$. Skipping prefactors of order of unity, $\tau' = \rho r^2/\mu$. Thus the sedimentation velocity $v_\infty \propto \Delta\rho g r^2/\mu$ is reached for times much longer than τ'. In this situation, the break up occurs before that the transient duration τ' is over, so that v_∞ is never reached. By this observation, it is shown that $\tau_1 = r/v_\infty$, which is the time for the transfer of v_∞ across the drop radius, serves as the minimum time for the formation of the vortex ring. The subsequent break up time τ_{bu} is longer than τ_1 and less than τ' and τ_2. Exploring further the fragmentation process , we have that for $\tau' << \tau_1$ the ring disappears by diffusion, while for $\tau' > \tau_1$ the torus experiences local perturbations coming from the increasing velocity. As a consequence, the ratio [5]

$$T = \frac{\tau_1}{\tau'} = \frac{\mu^2}{g\rho\Delta\rho V} \tag{2}$$

is decreased and there is increasing number of individual horizontal fragments associated with the first break up. By relating the diffusion time τ_2 to the equilibration time τ', the ratio

$$S = \frac{\tau_2}{\tau'} = \frac{\mu}{\rho D} \tag{3}$$

can be defined as the second characteristic non dimensional number of the problem. This coincide with the Schmidt number, which depends only on the fluid properties [5]. One can control one of the fluid parameters in such a way that when τ' is increased and S decreased, then the number of the horizontal fragments would increase.

2.2. The drop fragmentation and fractal process

In order to understand the self-similar process of the drop fragmentation, the same experimental set up as in Fig. 1 was used, but illuminating horizontally across the solvent with a collimated argon ion laser beam shaped as a thin lamina (500 μm) by means of a cylindrical lens. By changing the height of the lamina, the drops at different times and heights were followed. Beneath the cell is placed a plane mirror at an angle of 45°, that reflects the fluorescence induced by the passage of the drop through the two-dimensional slice of light. The drop break up at different cell heights is ruled by the fluid parameters and the cell is large enough to exclude the influence of the lateral boundaries. Using different drop volumes, a series of sectional images ranging from 64x64 up to 320x320 pixels and recorded at ten different successive heights and times were analyzed. Each digitized image contained levels of the normalized intensity varying from 0 to 255.

Using a drop of volume 2 μl, the height $h(t)$ versus time was plotted, as shown in Fig. 6. Three distinct regions can be distinguished, namely: region I indicates the initial drop fall, region II shows the fragmentation process and region III corresponds to the onset of diffusing droplets. We formulate a power law for the regions as $h \sim t_i^\gamma$ with γ_i being different exponents. By plotting the scaling exponents against drop volume as shown in Fig. 7, it can be deduced that $\gamma_i \sim V^x$ as follows: in region I, we have a relation of $\gamma_I \sim V^{0.50\pm0.02}$, in region II, $\gamma_{II} \sim V^{0.00\pm0.02}$ while in region III, $\gamma_{III} \sim V^{0.22\pm0.02}$. The second region, which is the fragmentation region, shows a universal behaviour

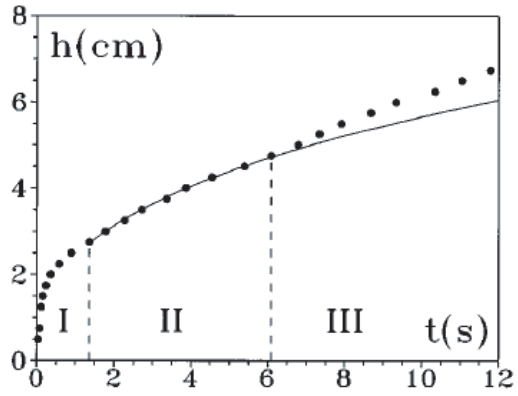

FIG. 6: Measured drop height as a function of the arrival time t, for an initial drop volume of 2 μl. The two vertical dashed lines mark the three regions identified as: I the first break-up region, ruled by the Fragmentation number F, II the fragmentation region, that depends on the Schmidt number S, and III the region of pure diffusion.

with an exponent $\gamma_{II} = 0.34 \pm 0.02$ independent from the initial drop volume.

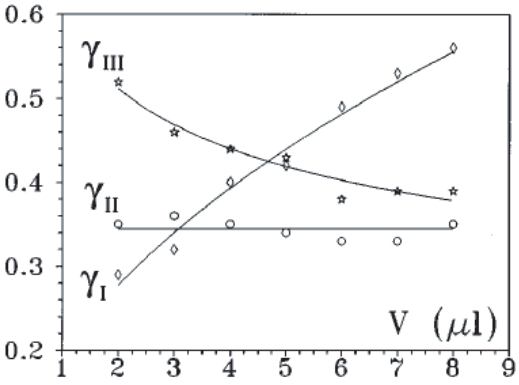

FIG. 7: Scaling exponents γ_I, γ_{II}, and γ_{III} of the height *vs* time $h \sim t^{\gamma}$ for the three different regions, respectively, as a function of the initial drop volume. The points are experimental data and the solid lines are best fits with $\gamma_I \sim V^{0.50\pm0.02}$ for the onset of the turban instability, $\gamma_{II} \sim V^{0.00\pm0.02}$ for the fragmentation region and $\gamma_{III} \sim V^{0.22\pm0.02}$ for the onset of diffusion. The second region shows a universal behaviour with an exponent $\gamma_{II} = 0.34 \pm 0.02$ independent from the initial drop volume.

Moreover, with the recorded digitized images and by using a box counting algorithm [6], we have computed the fractal dimension D_0 of the space occupied by the drop. The image space is partitioned into equally sized cubes of side ε. If $N(\varepsilon)$ is the number of cubes required to cover the space, the Renyi dimension can be calculated according to

$$D_q = lim_{\varepsilon \to 0} \frac{1}{q-1} \frac{\ln \sum_{i=1}^{N(\varepsilon)} p_i^q}{\ln \varepsilon} \tag{4}$$

Where, p_i is the image probability in the $i-th$ box defined as follows: in the discrete frame processing, we split the NxN pixels frame into mxm pixels boxes, where m specifies the discrete ε value selected. If we call $x(y)$ the horizontal (vertical) pixel coordinates, then the $i-th$ box will span the coordinates from x_i to x_i+m and y_i to y_i+m. Calling I_{xy} the intensity recorded at the pixel (x, y), the total signal is given by

$$I_t = \sum_{x,y=1}^{N} I_{xy} \tag{5}$$

whereas the local signal in the $i-th$ box is given by

$$I_i = \sum_{x=x_i}^{x_{i+m}} \sum_{y=y_i}^{y_{i+m}} I_{xy} \tag{6}$$

With this in mind we define as the image probability of the $i-th$ box the quantity

$$p_i = \frac{I_i}{I_t} \tag{7}$$

According to Eqn. (4), if log-log plots of $[\sum_{i=1}^{N(\varepsilon)} p_i^q]^{1/(q-1)}$ versus ε are plotted, the slopes of the linear regions correspond to D_q [7]. D_q are meaningful only in the range $-5 < q < 5$. D_q curves can be derived for different drops at different heights (such as $12, 22, 27, 32$ and 47 mm) for the fractalisation region and $(80, 110, 140, 170$ and 260 $mm)$ for the decreasing fractalisation region (diffusion). From the D_q curves, the $f(\alpha)$ curves were calculated with the Legendre transform [8] with $d = 2$ for two-dimensional sections of the flow by using the following expressions:

$$\begin{aligned} \alpha &= \frac{d}{dq}[(q-1)D_q] + 1 - d \\ f(\alpha) &= q(\alpha - 1 + d) - (q-1)D_q \end{aligned} \tag{8}$$

The function $f(\alpha)$ describes how densely a singularity of strength α is distributed over the analyzed set. Thus, $f(\alpha)$ can also be seen as the fractal dimension of the subset over which the singularities scale as α. A set characterized by a spectrum

of these dimensions is called multifractal since it can be thought of as constituted by many fractal subsets [9]. A plot of $f(\alpha)$ versus α curves were done [10] for different height regions (h from 12 to 47 mm) and (h from 80 to 260 mm) of the drop sections for a drop volume of 4 μl. From these curves, the fractal dimension D_0 of each image was deduced from the maximum of $f(\alpha)$ versus α plot. A plot of the measured fractal dimension D_0 as a function of the cell height h is shown in Fig. 8.

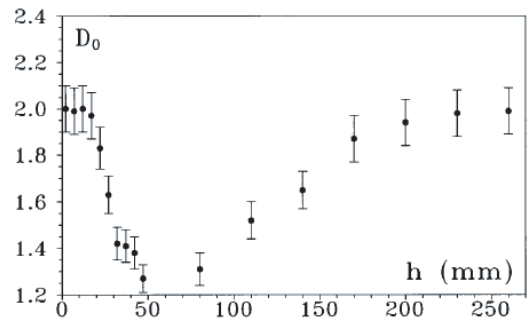

FIG. 8: Measured fractal dimension D_0 as a function of the cell height h, with initial drop instability at the (torus) and final stages (diffusion) with dimension of about 2. The dip of the curve shows the fractalization region.

In Fig. 8, it is observed that $D_0 = 2$ when the drop is whole up to torus whereas at the onset of fractalisation D_0 reduces to 1.3. Once the fractalisation is over and inhibited by diffusion, a reverse process, leading to the restoration of the dimension $D_0 = 2$, takes place. This reverse process for height inside the cell (h from 80 to 260 mm) is slow over a larger range. Similar results are obtained for different drop volumes. Thus, the drop fragmentation is a transient fractal taking place before the establishment of pure mixing between drop and solvent. The fragmentation cascade seems to share some generic properties of self- similar processes [10].

2.3. Interfacial surface tension and drop dynamics

The role of the initial surface tension of the drop against air is investigated, showing a strong release of energy from the rupture of the interface when the drop enters inside the solvent. Different fluid compositions, that is, $0, 10, 20, 35$ and 52% of glycerin for different initial drop volumes at room temperature $20\,^{\circ}C$ are used. The lateral and transverse images are recorded and combined through a video mixer so that both lateral and bottom views are simultaneously displayed, showing the height h reached by the ring and its radius R, as represented in Fig. 9 [11].

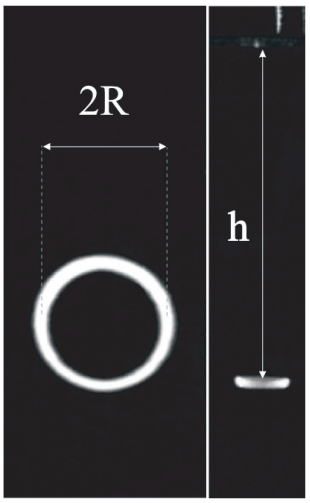

FIG. 9: Side and bottom image of the ring stop.

In order to deduce the height at which the ring stops, we use the energy balance between the surface energy, $4\pi\sigma r^2$, and the kinetic energy $4/3\pi r^3\rho v_0^2/2$, thus giving an expression as $\sigma r^2 = (\rho r^3 v_0^2)/6$. Once the initial velocity v_0 is acquired, $v_0 = (6\sigma/\rho r)/2$, we account for the energy dissipation through the Stokes law so that $dv/dt = -\gamma\nu v/r^2$ where $\gamma = 6\pi$ is the shape factor for a rigid sphere. Integrating the Stokes law for $v(t)$ and the maximum height h reached by the drop, we have

$$h = \frac{1}{\gamma}\sqrt{\frac{\sigma}{\rho\nu^2}}V^{\frac{1}{2}} \propto l_\nu^{-\frac{1}{2}} r^{\frac{3}{2}} \tag{9}$$

Where, $l_\nu = \rho\nu^2/\sigma$ is the viscous length scale. By substituting for σ, ρ and ν, the values tabulated in the current literature [12], we obtain a good quantitative agreement between the model and the experimental results. Note that r is proportional to $V^{1/3}$ where V is the initial drop volume.

To compare the effect of the surface tension, the experiment was performed also by using ethanol, which is a fluid of lower viscosity and much lower surface tension than the mixtures of water/glycerin. A plot of h versus V is shown in Fig. 10, whereas R versus V is shown in Fig. 11 [11]. In Fig. 10 all the data scales as $V^{1/2}$, whereas two scaling regions depending on the drop volume and viscosity observed in Fig. 11. For small volumes and large viscosities the exponent of the power law

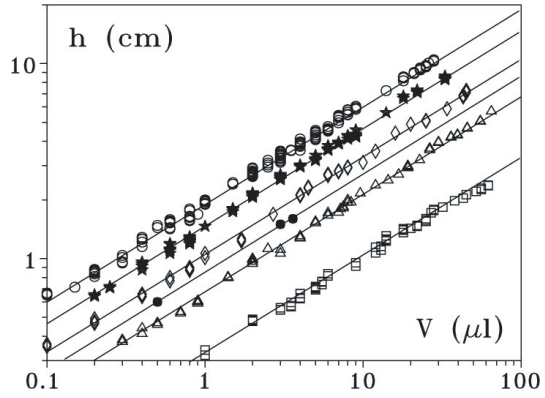

FIG. 10: Drop height h as a function of the initial drop volume V for different fluid compositions; empty circles: pure water, stars: 10% glycerine in water (Gly), diamonds: 20% Gly, triangles: 35% Gly, squares: 52% Gly, filled circles: pure ethanol.

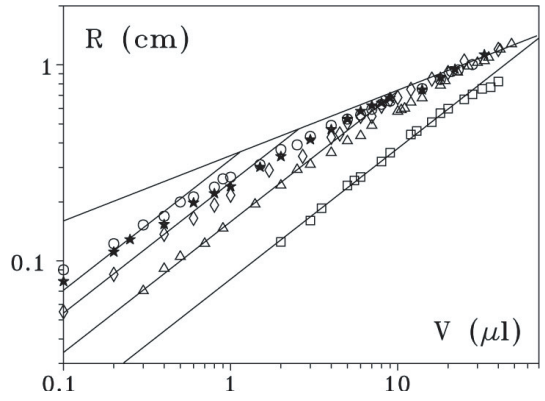

FIG. 11: Drop radius R as a function of the initial drop volume V for different fluid compositions; empty circles: pure water, stars: 10% Gly, diamonds: 20% Gly, triangles: 35% Gly, squares: 52% Gly. Solid lines have two slopes, namely, 2/3 and 1/3. Each separate data set displays a smooth passage from 2/3 to 1/3 slope as V increases.

fit the data with 2/3, while for large volumes and smaller viscosities the exponent approaches 1/3. The 1/3 and 2/3 scalings correspond to two asymptotic behaviours, the separation between them depending on the fluid parameters.

Such observations reveal that the surface tension σ of the droplet against air plays a fundamental role in the initial stage of the dynamics of a drop falling in a miscible fluid [13]. For zero density difference between the drop and the solvent, we have shown that the velocity at which the drop enters the fluid is proportional to the square root of the surface tension and thus the dissipation viscous length l_ν permits the rescaling of the data for height and drop volume to universal power law behaviours.

2.4. Path reversal of the falling drop

Several experiments with solvent heavier than the drop were performed by changing the drop volume and the density difference $\Delta\rho$. In each case the drop evolution was recorded by a CCD camera into frames binarized and processed. On each frame, the coordinates are noted by following the trajectory until the drop stops its descent and starts rise up, breaking into fragments. By selecting one fragment out of the many, its motion is followed by recording the coordinates of its centre of mass. The evolution of the longitudinal coordinate h of the centre of mass is plotted as a function of time for a fixed drop volumes, $V = 4\ \mu l$, and for different $\Delta\rho$ as shown in Fig. 12 and for a fixed $\Delta\rho = 0.04505$ g/cm^3 and different drop volumes, $V = 2, 4, 6, 8\ \mu l$ as shown in Fig. 13.

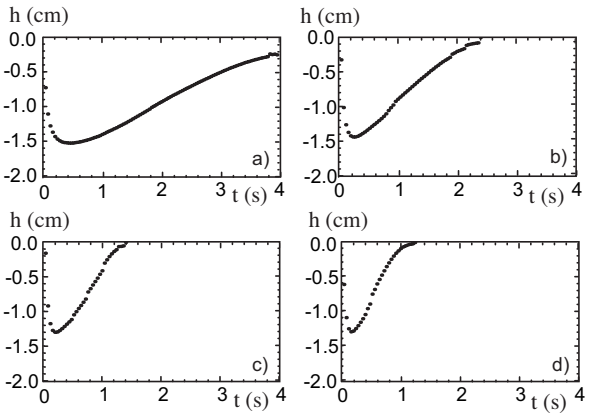

FIG. 12: Drop height profile as a function of time for $V = 4$ μl; $\Delta\rho =$ a) 0.01325, b) 0.0265, c) 0.03975, and d) 0.04505 g/cm^3

From Fig. 12 and Fig. 13 we can see that, once the drop has evolved into a vortex, it stops at a minimum height h_{min}, which is ruled by the initial drop volume V. On the other hand, when fragmentation takes place, the rise-up time for secondary droplets mainly depends on the density difference $\Delta\rho$, eventually going to infinity for $\Delta\rho = 0$. At small $\Delta\rho$, the rise-up time is very long, while it shortens as $\Delta\rho$ increases. The dynamical behavior of the drop accounts for buoyancy and viscous dissipation and is given by

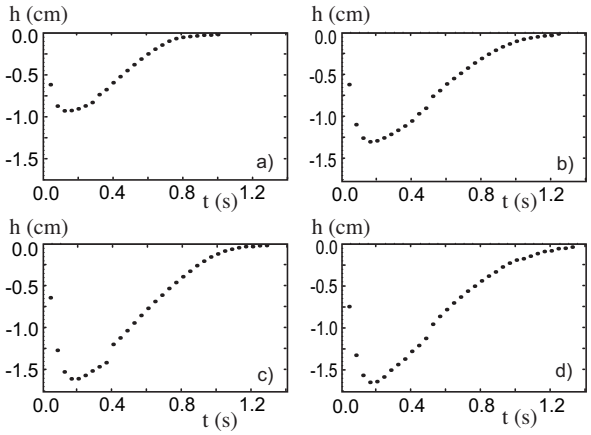

FIG. 13: Drop height profile as a function of time for $\Delta\rho = 0.04505\ g/cm^3$; V = a) 2, b) 4, c) 6, and d) 8 μl.

$$\frac{dv}{dt} = \frac{g\Delta\rho}{\rho} - \gamma\frac{\nu}{r^2}v \tag{10}$$

Where, $r = \kappa\sqrt[3]{V}$ and γ, κ are geometrical factors ($\gamma = 9/2$ and $\kappa = 0.62$ for a sphere [2]). The initial condition for the drop injection is given by $v(t = 0) = v_0$, where v_0 comes from the conversion of the drop surface tension into kinetic translational and rotational energy expressed as

$$\frac{1}{2}mv_0^2 + \frac{1}{2}I\omega^2 = 4\pi\sigma r^2 \tag{11}$$

with $I = \alpha mr^2$ the inertial momentum of the drop and $\omega = \beta v_0/r$ its frequency of rotation. If all the rotation is converted into translation, i.e., there is no sliding, then $\beta = 1$, otherwise $\beta > 1$. We obtain for the initial velocity of the drop

$$v_0 = -\sqrt{\frac{6\sigma}{(1+\alpha\beta^2)\rho r}} \tag{12}$$

Taking the viscous time $\tau_\nu = r^2/\gamma\nu$, we derive from Eqn. (10) the drop asymptotic velocity, v_∞ when $dv/dt = 0$, as

$$v_\infty = \frac{\Delta\rho}{\rho}g\tau_\nu \tag{13}$$

Integrating Eqn. (10) from $v = v_0$ to $v = 0$ the drop fall-down time, τ_d, is deduced as

$$\tau_d = \tau_\nu \ln(1 - \frac{v_0}{v_\infty}) \tag{14}$$

and the minimum height, h_{min}, reached by the drop before rising-up is expressed as

$$h_{min} = v_\infty\tau_d + v_0\tau_\nu \tag{15}$$

The fragment rise-up time τ_u, if $t \gg \tau_\nu$ it is given by

$$\tau_u = -\frac{h_{min}}{v_\infty} = \mid \frac{v_0}{v_\infty} \mid \tau_\nu - \tau_d \tag{16}$$

with the total elapsed time is

$$\tau_T = \mid v_0/v_\infty \mid \tau_\nu \tag{17}$$

Where, n is the number of fragments. Rescaling the $h-t$ data by h_{min} and τ_T, the reduced profile is plotted as h/h_{min} versus t/τ_T as shown in Fig. 14.

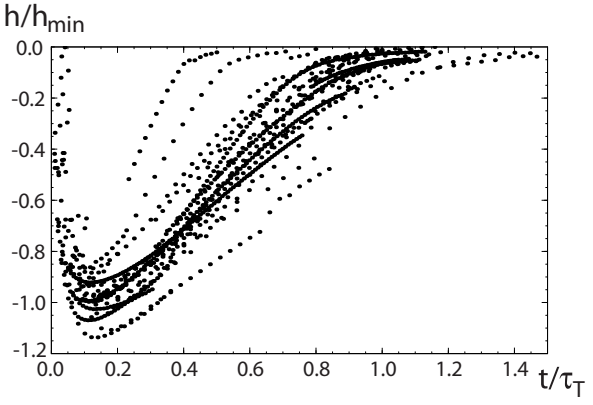

FIG. 14: Reduced $h - t$ profiles for all the experiments in 25% glycerine doped solvent.

All the drops approximately follow the same evolution law. The early stages of the drop injection are very similar to those observed at $\Delta\rho = 0$: the drop falls very fast inside the solvent and develops a ring. Then, the ring stops because of dissipation of the initial impulsion. The drop is said to reach its minimum height h_{min}, where a velocity reversal occurs giving way to a new instability that leads to the fragmentation of the ring into smaller droplets. With the density difference being negative, the secondary droplets rise up towards the surface because of buoyancy. Thus, the dynamical regime corresponds to the linear portions of the $h - t$ profiles just after h_{min}. These drop fragments, when approaching the free surface of the solvent, deviate from the linear dependence [14].

3. Conclusions

In summary, the physics of liquid drops needs to be unveiled in order to have more relevant practical applications in agriculture and industry [15]. The experimental characterisation of the dynamical and statistical features of a drop falling in a lighter miscible fluid can serve this purpose. The process can be associated with three dynamical regions, one corresponding to the onset of the torus and the first hydrodynamic instabilities, the other characterised by the successive fragmentation of the initial drop into smaller droplets and the last one dominated by diffusion, in which the droplets mix with the solvent without undergoing further fragmentations. The drop dynamics is ruled by three characteristic times through which two non-dimensional numbers, namely the Fragmentation number F and the Schmidt number S, were derived. While the first region of the drop becoming a torus is ruled by F, the fragmentation region of successive break-up is determined by S. In order to understand the development of the torus at the early stages of the drop before rupture, further experiments were performed on the role of the interfacial tension and its dissipation energy. The initial stage of the drop injection was found to be independent of the density difference between the drop and the solvent being either positive or negative. In the fragmentation region, the fractalization can be attributed to a multifractal structure of the droplet projections at different height. By using scaling laws on the drop volume V and various height h reached before the formation of the torus and also during the fragmentation process, h and V can be rescaled to universal power law behaviours.

Acknowledgments

P. K. B-B acknowledges the Abdus Salam International Centre for Theoretical Physics (ICTP), Trieste, for financial support under the Associate Scheme, TRIL programme, and the Office of External Activities. P.K.B-B is also indebted to Istituto Nazionale di Ottica Applicata, Italy and Institut Non-Lineare de Nice, France for hosting the experiments.

References

[1] J. J. Thomson and H. F. Newall, Proc. R. Soc. London **39**, 417 (1885).

[2] D. J. Tritton, *Physical Fluid Dynamics*, second edition (Clarendon Press, Oxford, 1988).

[3] H. Helmholtz, Berl. Mber. **215** (1868); also Philos. Mag. **36**, 337 (1868).

[4] F. T. Arecchi, P. K. Buah-Bassuah, F. Franchini, C. Perez-Garcia and F. Quercioli, Europhys. **9**, 333 (1989).

[5] F. T. Arecchi, P. K. Buah-Bassuah and C. Perez-Garcia, Europhys. Lett. **15**, 429 (1991).

[6] H. Froechling, J. P. Crutchfield, D. Farmer, N. H. Packard and R. Shaw, Physica D **3**, 605 (1981).

[7] R. R. Prasad, C. Meneveau and K. R. Sreenivasan, Phys. Rev. Lett. **61**, 76 (1988).

[8] T. C. Hasley, M. H. Jensen, L. P. Kadanoff, I. Procaccia and B. I. Shraiman, Phy. Rev. A. **33**, 1141 (1986).

[9] J. Feder, *Fractals*, (Plenum, New York, 1988).

[10] F. T. Arecchi, P. K. Buah-Bassuah, F. Francini and S. Residori, Phys. Rev. E. **54**, 424 (1996).

[11] S. Residori, E. Pampaloni, P. K. Buah-Bassuah and F. T. Arecchi, Eur. Phys. J. B. **15**, 331 (2000).

[12] R. C. Weast, *Handbook of Chemistry and Physics* (The Chemical Rubber Co., Cleveland, Ohio, 1971).

[13] M. Kojima, E. J. Hinch and A. Acrivos, Phys. Fluids **27**, 19 (1984).

[14] P. K. Buah-Bassuah, R. Rojas, S. Residori and F. T. Arecchi, Phys. Rev. E. **72**, 1 (2005).

[15] See e.g., J. Eggers, Rev. Mod. Phys. **69**, 865 (1997).

Received: 28 September, 2012
Accepted: 14 March, 2014